Influence of sea surface temperature on the intraseasonal variability of the South China Sea summer monsoon

Mathew ROXY[1,2] and **Youichi TANIMOTO**[2,3]

[1]*Indian Institute of Tropical Meteorology, Pune, India*

[2]*Faculty of Environmental Earth Science and Graduate school of Environmental Science, Hokkaido University, Sapporo, Hokkaido, Japan*

[3]*Research Institute for Global Change, JAMSTEC, Yokohama, Kanagawa, Japan*

Keywords: South China Sea, Asian monsoon, Ocean atmosphere interaction, Intraseasonal variability

Citation: Roxy M. and Y. Tanimoto, 2011: Influence of sea surface temperature on the intraseasonal variability of the South China Sea summer monsoon. Climate Dynamics, 39 (5), 1209-1218, DOI: 10.1007/s00382-011-1118-x

---

Corresponding author address: Mathew Roxy, Centre for Climate Change Research, Indian Institute of Tropical Meteorology, Pune 411008, India. E-mail: roxy@tropmet.res.in

Abstract

The objective of this study is to examine, based on recently available high resolution satellite and observational data, the evolution and role of sea surface temperature (SST) in influencing the intraseasonal variability of the South China Sea (SCS) summer monsoon (SM). The study focuses on the 30-60 day timescale when the northward propagating anomalies are dominant over the SCS. Composite analysis of the SST maximum events during SCS SM shows that increased SST anomalies over the SCS are significantly influenced by the downward shortwave radiation flux anomalies, with the suppressed surface latent heat flux anomalies supplementing to it. A thermal damping of the positive SST anomalies induces positive upward heat fluxes, which then destabilize the lower atmosphere between 1000hPa and 700hPa. The positive SST anomalies lead the positive precipitation anomalies over the SCS by 10 days, with a significant correlation (r=0.44) between the SST-precipitation anomalies. The new findings here indicate an ocean-to-atmosphere effect over the SCS, where underlying SST anomalies tend to form a favorable condition for convective activity and sustain enhanced precipitation during the SCS SM. It is also argued, based on our observations, that the negative sea level pressure anomalies induced by the positive SST anomalies play a role in enhancing the northward propagation of the intraseasonal anomalies over the SCS.

1. Introduction

The South China Sea (SCS), the largest marginal sea in the western North Pacific Ocean, is overlaid by a pronounced monsoon surface wind. The Indian and East Asian monsoon systems interact over the SCS region (Chen and Chen 1995; Lau et al. 1998; Mao and Chan 2005). In addition, the onset of the SCS summer monsoon (SM) indicates the onset of the East Asian summer monsoon (Tao and Chen 1987; Murakami and Matsumoto 1994; Wu and

Wang 2000, 2001) and hence it is of significant interest to understand the intraseasonal variability of the SCS SM.

Intraseasonal variability of the SCS SM involves two intraseasonal time scales in the periods ranging from 10 to 20 days (Krishnamurti and Ardanuy 1980) and 30 to 60 days (Murakami et al. 1984; Krishnamurti and Subrahmanyam 1982; Lau and Peng 1987). The 10-20-day time scale is observed to exhibit dominant westward propagation while the 30-60-day time scale is observed to exhibit dominant northward propagation (Chen and Chen 1993; Chen and Chen 1995). An examination of the intraseasonal variability based on the data from South China Sea Monsoon Experiment (SCSMEX), showed that these two intraseasonal time scale influence the maintenance and break of the SCS SM (Chan et al. 2002). Mao and Chan (2005), using NCEP-NCAR reanalysis data, found that both of the time scales are distinct, that they do not always exist simultaneously in a particular year, and their contributions to the overall variations differ among different years. They also found that for the years when both time scales are present, the SCS SM activities are basically controlled by the 30-60 day time scale, though modified by the 10-20 day time scale. Isoguchi and Kawamura (2006) observed significantly large covariance in the SST anomalies and a 30-60 day intraseasonal variability index based on zonal winds and outgoing longwave radiation over the western SCS.

Several of the studies dealing with the SCS SM have explored the atmospheric variability involved in the intraseasonal variability and its northward propagation characteristics, but only a handful of studies have examined the role of the underlying SST on it (eg: Xie et al. 2007; Wu 2010). Understanding the SST-precipitation relationship and the ocean-atmosphere processes involved in it is crucial for evaluating and rectifying model forecasts (Wu et al. 2006, 2008). For example, Wu et al. (2008) using local SST-precipitation relationship found out discrepancy between an ocean-atmosphere coupled model and observations with the SST

lag time longer in the model than in observations. This was attributed to a slower SST response to atmospheric changes in the model, as compared to observations.

Kemball-Cook and Wang (2001) attempted to evaluate the processes involved in the northward propagating intraseasonal anomalies over Indian Ocean and western tropical Pacific. They suggested that, over these regions, the negative latent heat flux (upward negative) anomalies enhance the northward propagating convective anomalies through an increase in the moist static energy. A study on the thermodynamics involved in the northward propagating anomalies over the Indian Ocean was carried out by Roxy and Tanimoto (2007) using satellite data based on the Tropical Rainfall Measuring Mission (TRMM). They found that, over the off-equatorial regions, the underlying SST anomalies induce unstable conditions in the lower atmosphere and enhance the northward propagating precipitation anomalies. The climatological features of the SCS region are comparable to that of the north Indian Ocean. During the summer monsoon, surface winds over the SCS region are southwesterly (Fig. 1a) as over the Indian Ocean. Also, the mean SST during this period is above 27°C (Fig. 1a), which is conducive for enhanced convective precipitation (Lau et al. 1997). Sengupta et al. (2001) showed that SST intraseasonal variability over the SCS is among the highest over the tropics. Hence understanding the ocean-atmosphere interactions involving SST during the SCS SM on intraseasonal timescales is of paramount importance.

Fu et al. (2008), using ensemble forecasts from five different lower boundary conditions, by changing the coupling between the atmosphere and ocean, pointed out that positive intraseasonal SST anomalies in the western Pacific Ocean trigger convective disturbances by moistening and warming up the atmospheric boundary layer. The role of intraseasonal SST anomalies in assisting the convection, particularly for the SCS SM onset, was examined by Wu (2010) by analyzing satellite observations along with reanalysis data. Their study indicated that the northward propagation of these SCS SM intraseasonal anomalies is related

to the ocean–atmosphere interaction, involving the wind-evaporation and cloud-radiation effects on SST as well as SST impacts on lower-level convergence over the equatorial western Pacific and atmospheric instability over the Philippine Sea and the South China Sea. Zeng and Wang (2009) estimated latent heat flux anomalies from TRMM satellite SST, wind speed and total precipitable water, and revealed northward propagation of latent heat flux anomalies over the SCS, which they attributed as a response to the northward propagating intraseasonal anomalies within the 30-60 day timescales.

Wu (2010) focuses on the onset of the SCS SM, and consider both the 10-20 and 30-60 day intraseasonal time scales together in their analysis. Studies, however, show that the propagation and evolution of monsoon intraseasonal signals are distinct and that they undergo different ocean-atmosphere interaction due to their contrasting temporal evolutions (Kajikawa and Yasunari 2005; Mao and Chan 2005; Zheng et al. 2004). Due to the crucial part played by the SCS SM intraseasonal anomalies in the East Asian summer monsoon, it is imperative that a role of ocean in influencing the northward propagating monsoon intraseasonal anomalies, that is in the 30-60 day time scales, during the whole period of the SCS SM is investigated. Examining this role, and providing a step by step process of the ocean-atmosphere interaction involved, is the primary objective of the present work. Also, the earlier studies which established some observational evidence for the role of ocean on intraseasonal monsoon anomalies (Roxy and Tanimoto 2007; Wu 2010), depend heavily on the NCEP Reanalysis II for the surface variables such as the heat fluxes, winds and air temperature. This model-dependence will essentially cause an over-matching relationship among these variables and possibly over-estimate the local ocean atmosphere relationship to a large degree. In the present study we use real observation based latent heat and shortwave fluxes, and surface satellite winds, thus considerably improving the quality of the analysis.

Wang and Wu (1997a) showed that, from May to July, the intraseasonal variability of SCS SM is primarily associated with a northward propagation of the intraseasonal anomalies from the equator to 25°N. Recent studies (eg: Wu 2010) indicates the occurrence of intraseasonal anomalies along with the monsoon onset, in April also. Hence, we examine the intraseasonal SCS SM variability during April to July over the SCS domain 5°S-25°N, 105-125°E, where the northward propagating intraseasonal anomalies are most significant.

2. Data and analysis methods

This study examines a suite of new high resolution satellite observations of SST, sea surface wind, and precipitation and objective analysis of latent heat and shortwave fluxes. The fact that these high quality datasets are available for the last 12 years (since the year 1998) helps us in analyzing significantly large number of intraseasonal events, improving the confidence in the present results.

The 3-day running mean SST and precipitation based on the TRMM Microwave Imager (TMI) on 0.25° grid, from the year 1998 to 2009 is used in this study. Using microwave sensors, TMI measures SST and surface wind speed nearly free of cloud influence over the tropical-extra tropical regions within 38°N/S, with a spatial resolution of 0.25°and temporal resolution of 2~3 days (Wentz et al. 2000). This substantially improves the sampling of SST over cloudy regions like SCS during summer (Xie et al. 2001). Many studies have used outgoing longwave radiation (OLR) values to examine the development of SCS SM (eg: Mao and Chan 2005) while an improvement in the present study is that the TMI precipitation is used.

Sea surface winds are obtained from the microwave scatterometer on the QuikSCAT satellite which measures surface wind velocity over the world ocean on a daily basis on a 0.25° grid (Liu et al. 2000). The QuikSCAT observations are available from August 1999

only. The European Remote Sensing (ERS) scatterometer, though at a coarser resolution (1° grid), provides surface wind observations for a longer period, and hence is blended to make a daily surface wind dataset for the years 1998 to 2009 for consistency with the other datasets.

The surface latent heat flux (SLHF) data is obtained from the Objectively Analyzed Air–Sea Fluxes (OAFlux) project (Yu et al. 2008), an optimal blending of multi-platform satellite retrievals and numerical weather prediction reanalyses and the downward shortwave radiation flux (DSWRF) is obtained from the International Satellite Cloud Climatology Project (ISCCP), both at 1° grid with a temporal resolution of 1 day. The satellite and observed fields are supplemented with daily air temperature, specific humidity and sea level pressure (SLP) at 1.5° grid based on the European Centre for Medium- Range Weather Forecasts (ECMWF) Interim (ERA-Interim) reanalysis. The lower tropospheric air temperature and specific humidity is used to derive the equivalent potential temperature (θ_e), which is a useful parameter in understanding the atmospheric stability. The lower tropospheric stability is estimated as a difference in θ_e between 1000hPa and 700hPa, following Roxy and Tanimoto (2007).

Data of SST and precipitation between April 1 and July 31 from 1998 to 2009 are interpolated to daily for compatibility among variables. Anomalies are obtained for all variables by removing the seasonal means for each of individual years. These anomalies are band pass filtered for 30-60 days to retain the northward propagating intraseasonal anomalies over the SCS. These intraseasonally filtered anomalies are used in the present study.

3. Results

3.1. Intraseasonal variability and SST-precipitation relationship in the SCS

To analyze the regional characteristics of intraseasonal variability over the SCS, we plot the summertime standard deviations (April to July) of intraseasonal SST variability in

Figure 1b. Large standard deviations of the intraseasonal variability emerge over the central-western SCS (107-114°E, 9-12°N). The significantly large standard deviation over this region can be attributed to the upwelling over this region due to the strong monsoon winds during boreal summer (Xie et al. 2003). This is similar to the region of large covariance observed by Isoguchi and Kawamura (2006; 109-114°E, 9-12°N) at periods of 30–60 days during June to September. In the present study, we observe standard deviations of similar magnitude over the northeastern SCS also. Due to its pivotal position, we utilize the central part of SCS with large SST variability in the inset rectangle over 109-114°E, 9-12°N (Fig. 1b), to examine the development and sustenance of intraseasonal SST and precipitation over SCS SM. This will help in getting a better perspective of the intraseasonal anomalies along with the evolution and degeneration of the SST anomalies, and any associated propagation of the intraseasonal anomalies from south to north.

The time series of the SST and precipitation anomalies averaged over the above region, from April-July, for the years 1998-2009 is shown in Figure 2. It is evident that the two time series are coherent at ~90° phase. The positive SST anomalies clearly lead the precipitation anomalies during all the years, though the relationship appears to be slightly weaker in the beginning of the SCS SM each year. To elucidate the relationship further, the lead-lag correlations of the SST anomalies with respect to the precipitation anomalies over the same region are estimated from 20 days before to 20 days after, over the 12 year period for the SCS SM (Fig. 3). A positive correlation observed when SST leads the precipitation anomalies indicates that the SST is driving the atmosphere, which is denoted as an ocean-to-atmosphere effect (Roxy and Tanimoto 2007; Wu et al. 2008). A negative correlation when SST lags the precipitation anomalies implies that the atmosphere is driving the SST, which is denoted as an atmosphere-to-ocean effect. The magnitude of the maximum (minimum) correlation denotes the intensity of the ocean-to-atmosphere (atmosphere-to-ocean) effect,

and the corresponding lead (lag) time denotes how quickly the atmosphere responds to the SST anomalies and vice versa.

The correlation is nil and insignificant when the SST and precipitation are correlated with a 0 day lag, and increases with the lead/lag. This indicates that the SST-precipitation relationship is not an instantaneous one, but on a lead/lag of several days. Maximum positive correlation (r=0.44, at 99% significant levels) is observed when the SST leads the precipitation by 10 days. This suggests that ocean-atmospheric processes induced by the intraseasonal SST anomalies results in enhanced precipitation during the SCS SM. Maximum negative correlation (r=0.39, at 99% significant levels) is obtained when the SST lags the intraseasonal precipitation anomalies by 12 days, suggesting an ocean cooling as a response to increased cloudiness associated with the precipitation.

3.2. Evolution of intraseasonal SST anomalies during the SCS SM

To examine the temporal evolution of the SCS SM intraseasonal variability with respect to the intraseasonal SST anomalies, we define an SST maximum (SST max hereafter) event as the days when the positive SST anomalies in the region (Fig. 1b, Fig. 2) exceeds a threshold value of 1 standard deviation (0.242°C), representing strong anomalous intraseasonal variability. Most of the SST max events sustain for an average duration of ~12 days. Eighteen (18) events of SST max are identified during 1998-2009. Composites of all variables, for all the ±20 days with respect to the SST max are prepared. This period (41 days) roughly includes the evolution and sustenance of the positive SST anomalies (12+ days) and the processes leading to the positive precipitation anomalies (10 days).

Latitude-time plots of daily composite variables averaged over the region of 105-125°E are shown in Figure 4. Coherent northward migrations of the anomalies over the SCS are observed from the equator towards the northern SCS, up to 25°N. The average propagation

speed of the anomalies, from 0° to 20°N, is about 1.0° latitude per day (20° per 20 days). Figures 4a to 4d shows the variables and processes involved in the evolution of positive SST anomalies. It is observed that the anomalous easterly surface winds (Fig. 4a) which oppose the climatological southwesterlies (Fig. 1a) induce reduced evaporative cooling as shown by positive SLHF anomalies (Fig. 4b, ~10 W m^{-2} and downward positive). Positive DSWRF anomalies (Fig. 4c, ~14 W m^{-2}) appear at the same time, with intensity greater than the SLHF anomalies, warming the ocean surface. The positive DSWRF anomalies are as a result of a clearer sky, indicated by the negative precipitation anomalies in Figure 4h. On comparison, the SLHF anomalies are less prominent over the off-equatorial regions, and do not exhibit considerable northward propagation. Positive sensible heat net flux and net longwave radiation flux anomalies were also observed to be in phase with the other surface heat fluxes but they are too small in comparison and hence not shown here. This suggests that DSWRF and SLHF anomalies contribute to the evolution of positive SST anomalies (~0.4°C, contours in Fig. 4) with the DSWRF anomalies playing significant role over the off-equatorial region. The SST anomalies appear to show a comparatively slower propagation with respect to the winds and other intraseasonal anomalies. This can be attributed to the fact that, other than the DSWRF anomalies with prominent northward propagation, the SLHF anomalies with a slower northward propagation also contribute to the formation of SST anomalies.

The extent to which the surface heat flux anomalies can account for the observed intraseasonal variations of SST were examined using the SST tendency equation

$$\frac{\partial T_s}{\partial t} = \frac{F_{tot}}{\rho c_p h}$$

where T_s is the SST, F_{tot} is the total heat flux, ρ is density of water, c_p is the specific heat of water at constant pressure, and h is the mixed layer depth (MLD). The thickness of the MLD is a key factor influencing SST. In the nearby western Pacific warm pool, where MLD is deep, water upwelled from the subsurface is not very much different in temperature from the

surface water, and as a result, ocean dynamics has little effect on the surface thermal structure (Qu et al. 1997) However, this does not seem to be the case in the SCS, where MLD is shallow and upwelling occurs intermittently throughout the year (Chao et al. 1996). As a result, over the SCS, MLD may reach up to 60 m in winter and shoal down to about 30 m during summer (Qu 2001). In the present study, we use the MLD averaged at 30 m for the SCS SM during April to July. With the MLD defined as above, the observed SST tendency varied coherently with those derived from the surface heat fluxes, both in amplitude and phase, indicating that the surface heat flux anomalies account for the observed SST variability. For instance, with an F_{tot} of 28 W m^{-2}, h of 30 m and standard values of ρ (1.024 gcm^{-3}) and c_p (3.898 $Jg^{-1}°C^{-1}$), the heat flux forcing estimated is in the order of 0.023°C day^{-1}. This is comparable to the SST variability of 0.027°C day^{-1}, estimated for an SST change of 0.8°C in 30 days.

3.3. Ocean-to-atmosphere effect over the SCS

To explore how the observed SST anomalies influence the SCS SM precipitation anomalies, composite maps of the intraseasonal SST, surface wind and precipitation anomalies with respect to SST max is shown in Figure 5. Ten (10) days before the SST max (Fig. 5g), weakly positive anomalies (~ 2mm day^{-1}) of precipitation are found in the south of the SCS. These precipitation anomalies propagate northward and begin to intensify (above 6mm day^{-1}), eventually triggering enhanced precipitation over the central SCS (Fig. 5i), 10 days after the SST max.

In the region of the enhanced precipitation anomalies, an anomalous convergence of surface winds is observed in the 10-15°N zonal band (Fig. 5d). Increased precipitation from 10 to 20 days after SST max is associated with the intensification of the surface convergence indicated by Figs. 5d and 5e. The intraseasonal surface wind anomalies over the central SCS

during the prior to SST max are northeasterlies (~1ms^{-1}), which results in reduced wind speed as the seasonal mean winds are southwesterly. This weak wind speed causes the positive SST anomalies by the reduced heat release from the ocean. At the same time, as a result of a clearer sky indicated by the negative precipitation anomalies during SST max, the incoming shortwave radiation also increases, supplementing to the SST anomalies (~0.4°C) over the same region, forming a meridional gradient with positive (negative) SST anomalies in the center (south) of the SCS (Fig. 5b). This is followed by the strengthening of the anomalous southwesterlies (~2ms^{-1}) in the central SCS (Fig. 5d).

Figures 4e to 4h shows the latitude-time plots of intraseasonal anomalies involved in the SST-precipitation relationship. Coherent northward migrations of the anomalies over the SCS are observed at a phase speed of 1° per day, from equator to about 25°N. The local SST maximum leads relative to the northward-migrating enhanced precipitation, indicating that a warm ocean surface induced by weak wind speed and increased solar radiation may contribute to a favorable condition of the convective activity as like in the tropics (Fig. 4h). The positive SST anomalies (0.2-0.4°C) lead the positive precipitation anomalies (4-6 mm day^{-1}) by about 10 days (Figs. 2, 4 and 5). Though less intensive, the negative SST and precipitation anomalies follow the positive anomalies, making an intraseasonal cycle of 40~50days. For simplicity, we will focus on the positive precipitation associated with the SST maximum.

During the SST maximum, both the SST and SAT anomalies are positive and exhibit northward propagation simultaneously (Fig. 4e). In addition, upward heat flux anomalies act as a thermal damping of the positive SST, indicating an ocean-to-atmosphere effect. Such an ocean-to-atmosphere effect induce the positive anomalies in $\Delta\theta_e$ (0.2°C) over the same region (Fig. 4g), a condition favoring convective activity. Indeed, θ_{e1000} anomalies were observed to be similar to the SAT anomalies (Fig. 4f). The positive $\Delta\theta_e$ anomalies render adequate

unstable condition before the precipitation maximum. The destabilization of the lower atmosphere may provide the uplift of the moisture content from the lower atmosphere and the consequent condensation resulting in positive cloud liquid water anomalies (not shown here), giving rise to enhanced precipitation. The positive precipitation anomalies lag SST by 10 days and coincide with the unstable condition in the lower atmosphere. These findings suggest an ocean-to-atmosphere effect, where SST anomalies enhance the convective clouds through changes in the vertical structures of the lower-tropospheric temperature and moisture content. The suggested ocean-to-atmosphere effect appears to work effectively over the central SCS, where the intraseasonal SST anomalies are significant.

4. Discussion and concluding remarks

Using observed SST, precipitation, surface wind, SLHF, DSWRF, SAT, SLP and equivalent potential temperature, we have analyzed the relationship between the northward propagating intraseasonal SST and precipitation during SCS SM. Coherent northward propagation of the anomalies are observed over the SCS at a phase speed of 1° per day, from the equator to 25°N. The anomalous surface easterlies against the mean westerly flow result in positive SLHF anomalies. The positive DSWRF anomalies and positive SLHF induced by reduced wind are observed to contribute to the evolution of positive SST anomalies. The DSWRF anomalies are more significant in inducing the observed SST variability over the off-equatorial regions of SCS. Meanwhile, a similar study of the ocean-to-atmosphere effect over the Indian Ocean during the Indian summer monsoon (Roxy and Tanimoto 2007) have shown that SLHF anomalies are more significant at similar latitudes. The comparatively shallow mixed layer depth of about 30m supplement to the observed SST variability during the SCS SM.

The northward propagating positive SST anomalies are found to induce an ocean-to-atmosphere effect near the sea surface, through a thermal damping of the positive SST. The positive SST anomalies are followed by the positive $\Delta\theta_e$ anomalies, suggesting the active role of SST anomalies in inducing unstable conditions over the lower atmosphere, which results in enhanced precipitation over the SCS at a lag of 10 days. Thus, the results presented herein suggest that SST anomalies over the SCS are significant in locally enhancing the northward propagating precipitation anomalies during the SCS SM. Even though the focus of the present study is only on the active (positive) phase of the intraseasonal cycle, it is found that the break (negative) phase also follows a similar process. The negative SST and precipitation anomalies follow the positive anomalies (not shown), making an intraseasonal cycle of 40~50 days.

Though the present study has dealt with the mechanism involving the ocean-atmosphere processes involved in enhancing the precipitation anomalies, one of the factors left unexplained is the change of the surface wind anomalies from easterlies to westerlies and vice versa. Previous studies (Matsuno 1966; Gill 1980; Wang and Wu 1997b) have examined the wind response to topical convective activity and have suggested possible mechanisms. These studies suggest that surface westerly anomalies are negatively correlated with OLR anomalies as a response of tropical atmosphere to convective heating. This is observed in the anomalous westerlies during the precipitation maximum (Figs. 5d, 5i; 10 days after SST max). Similarly, the suppressed convective activity during the precipitation minimum (Figs. 5b, 5g; 10 days before SST max) results in anomalous easterlies. However, the processes involved in the reversal of the surface wind anomalies require further investigation with respect to the present study. With the hypotheses and propositions provided here, a comprehensive picture of the active – break intraseasonal cycle of precipitation over the SCS is illustrated in Figure 6.

An additional role of the ocean, in enhancing the northward propagation observed in the anomalies, is further examined. The precipitation bands associated with the Asian monsoon

migrate from its mean winter location slightly south of equator to the mean summer location near 20°N, in association with the seasonal migration of the rising branch of the Hadley cell known as the intertropical convergence zone (Rao 1976; Sikka and Gadgil 1980). The northward propagation observed in the intraseasonal anomalies is super-imposed on this seasonal northward migration. Several studies have looked into the dynamics involved in this propagation over the Asian monsoon region (Goswami and Shukla 1984; Hsu et al. 2004; Jiang et al. 2004; Goswami 2005; Bellon and Sobel 2008; Chou and Hsueh 2010). In general, the origin of the northward propagation of the anomalies is associated with low-level convergence a few degrees north of the convection maximum. This low-level convergence could be caused by barotropic vorticity in the overlying atmosphere (Goswami 2005). Jiang et al. (2004) and Bellon and Sobel (2008) proposed different mechanisms for the low-level convergence associated with the barotropic vorticity. These studies indicate the predominant atmospheric variability associated with the northward propagating intraseasonal anomalies. Though the atmospheric variability may directly govern the essential dynamical process in the northward propagation, it is possible that the northward propagating anomalies are modulated by the ocean surface. Hence, it would be interesting to discuss the possibilities of a role of ocean, based on the results presented in this study.

Xie and Philander (1994) proposed a mechanism whereby a positive feedback of wind speed, evaporation and SST influence the meridional propagation of the anomalies over the tropics, with implications over the extra tropics (Xie and Tanimoto 1998). Similar to these studies, a role of the ocean in enhancing the northward propagation is observed in the anomalies, and is hypothesized as follows. The positive (negative) SST anomalies over the north (south) of SCS results in a meridional pressure gradient (Fig. 4d) as both are proportional, following Lindzen and Nigam (1987). The positive SST anomalies over the SCS are observed to create a region of negative SLP anomalies (Fig. 5j). North (south) of the SLP anomaly center, anomalous northeasterlies (southwesterlies) are observed. Under climatological southwesterlies, anomalous surface winds induce reduced (enhanced) upward

SLHF towards the north (south) of SST and SLP anomaly centers. This anomalous SLHF leads positive (negative) SST tendency north (south) of the SST and SLP anomaly centers, resulting in an enhancement of the northward propagation. However, it is important to note that a boundary layer model (eg: Lindzen and Nigam 1987) run with the observed SST changes does not reproduce the observed wind velocity changes. This inconsistency is generally owing to the problems in the representation of physics, especially those for the marine atmospheric boundary layer (Song et al. 2009). Hence, further improvement of the boundary layer in the model is necessary to elucidate whether the SST anomalies have an essential role in the northward propagation of the precipitation anomalies or a supportive role in the "enhancement" of the propagation through the modification of convective activity in the overlying atmosphere.

Acknowledgements

Constructive suggestions and comments from two anonymous reviewers have helped in improving the manuscript. NASA/GSFC are thankfully acknowledged for TMI/QuickScat satellite data. The latent heat flux data is obtained from the WHOI OAFlux Project and the downward shortwave radiation flux data from the International Satellite Cloud Climatology Project (ISCCP). The authors are thankful to the Centre for Climate Change Research at the Indian Institute of Tropical Meteorology, Ministry of Earth Sciences, India, for facilitating the study. This work was supported in part by the Global Environment Research Fund (S-5) of the Ministry of the Environment, Japan, Grand-In-Aid for Scientific Research defrayed by the Ministry of Education, Culture, Sports, Science and Technology of Japan (22340132, 22340135, 22106007).

References

Bellon G, Sobel AH (2008) Instability of the axisymmetric monsoon flow and intraseasonal oscillation. J Geophys Res 113:D07109

Chan JCL, Wi WX, Xu JJ (2002) Mechanisms responsible for the maintenance of the 1998 South China Sea Summer Monsoon. Journal of the Meteorological Society of Japan 80 (5):1103-1113

Chao SY, Shaw PT, Wu SY (1996) Deep water ventilation in the South China Sea. Deep-Sea Research Part I-Oceanographic Research Papers 43 (4):445-466

Chen TC, Chen JM (1993) The 10-20-Day Mode of the 1979 Indian Monsoon - Its Relation with the Time-Variation of Monsoon Rainfall. Monthly Weather Review 121 (9):2465-2482

Chen TC, Chen JR (1995) An Observational Study of the South China Sea Monsoon during the 1979 Summer - Onset and Life-Cycle. Monthly Weather Review 123 (8):2295-2318

Chou C, Hsueh YC (2010) Mechanisms of northward propagating intraseasonal oscillation-A comparison between the Indian Ocean and the western North Pacific. Bulletin of the American Meteorological Society

Fu X, Yang B, Bao Q, Wang B (2008) Sea Surface Temperature Feedback Extends the Predictability of Tropical Intraseasonal Oscillation. Monthly Weather Review 136 (2):577-597. doi:doi:10.1175/2007MWR2172.1

Gill AE (1980) Some simple solutions for heat-induced tropical circulation. vol 106. John Wiley & Sons, Ltd. doi:10.1002/qj.49710644905

Goswami BN (2005) South Asian monsoon. In: Lau KM, Waliser D (eds) Intraseasonal variability in the atmosphere-ocean climate system. Springer Berlin Heidelberg, pp 19-61. doi:10.1007/3-540-27250-x_2

Goswami BN, Shukla J (1984) Quasi-periodic oscillations in a symmetric general circulation model. Journal of the Atmospheric Sciences 41 (1):20-37

Hsu HH, Weng CH, Wu CH (2004) Contrasting characteristics between the northward and eastward propagation of the intraseasonal oscillation during the boreal summer. Journal of Climate 17 (4):727-743

Isoguchi O, Kawamura H (2006) MJO-related summer cooling and phytoplankton blooms in the South China Sea in recent years. Geophys Res Lett 33 (16):L16615. doi:10.1029/2006gl027046

Jiang XN, Li T, Wang B (2004) Structures and mechanisms of the northward propagating boreal summer intraseasonal oscillation. Journal of Climate 17 (5):1022-1039

Kajikawa Y, Yasunari T (2005) Interannual variability of the 10-25- and 30-60-day variation over the South China Sea during boreal summer. Geophysical Research Letters 32 (4):-

Kemball-Cook S, Wang B (2001) Equatorial waves and air-sea interaction in the Boreal summer intraseasonal oscillation. Journal of Climate 14 (13):2923-2942

Krishnamurti TN, Ardanuy P (1980) The 10–20-day westward propagating mode and breaks in the monsoons. Tellus 32:15-26

Krishnamurti TN, Subrahmanyam D (1982) The 30–50 day mode at 850 mb during MONEX. Journal of Atmospheric Science 39:2088–2095

Lau KM, Peng L (1987) Origin of low-frequency (intraseasonal) oscillations in the tropical atmosphere. Part I: Basic theory. Journal of Atmospheric Science 44:950–972

Lau KM, Wu HT, Bony S (1997) The role of large-scale atmospheric circulation in the relationship between tropical convection and sea surface temperature. Journal of Climate 10 (3):381-392

Lau KM, Wu HT, Yang S (1998) Hydrologic processes associated with the first transition of the Asian summer monsoon: A pilot satellite study. Bulletin of the American Meteorological Society 79 (9):1871-1882

Lindzen RS, Nigam S (1987) On the Role of Sea Surface Temperature Gradients in Forcing Low-Level Winds and Convergence in the Tropics. Journal of the Atmospheric Sciences 44 (17):2418-2436

Liu TW, Xie X, Polito PS, Xie S, Ping, Hashizume H (2000) Atmospheric manifestation of tropical instability wave observed by QuikSCAT and tropical rain measuring mission. Geophys Res Lett 27 (16):2545-2548. doi:10.1029/2000gl011545

Mao JY, Chan JCL (2005) Intraseasonal variability of the South China Sea summer monsoon. Journal of Climate 18 (13):2388-2402

Matsuno T (1966) Quasi-geostrophic motions in the equatorial area. J Meteor Soc Japan 44 (1):25-42

Murakami T, Matsumoto J (1994) Summer monsson over the Asian continent and western North Pacific. Hosei University, Department of Geography, Tokyo, JAPON

Murakami T, Nakazawa T, He J (1984) On the 40–50 day oscillations during the 1979 Northern Hemisphere summer. I: Phase propagation. Journal of the Meteorological Society of Japan 62:440–468

Qu TD (2001) Role of ocean dynamics in determining the mean seasonal cycle of the South China Sea surface temperature. Journal of Geophysical Research-Oceans 106 (C4):6943-6955

Qu TD, Meyers G, Godfrey JS, Hu DX (1997) Upper ocean dynamics and its role in maintaining the annual mean western Pacific warm pool in a global GCM. International Journal of Climatology 17 (7):711-724

Rao YP (1976) Southwest Monsoon. Meteorological Monograph. India Meteorological Department, New Delhi

Roxy M, Tanimoto Y (2007) Role of SST over the Indian Ocean in influencing the intraseasonal variability of the Indian summer monsoon. Journal of Meteorological Society of Japan 85 (3):349-258

Sengupta D, Goswami BN, Senan R (2001) Coherent intraseasonal oscillations of ocean and atmosphere during the Asian summer monsoon. Geophysical Research Letters 28 (21):4127-4130

Sikka DR, Gadgil S (1980) On the maximum cloud zone and the ITCZ over Indian longitudes during the southwest monsoon. Monthly Weather Review 108:1840-1853

Song Q, Chelton DB, Esbensen SK, Thum N, O'Neill LW (2009) Coupling between sea surface temperature and low-level winds in mesoscale numerical models. Journal of Climate 22 (1):146-164

Tao SY, Chen LX (1987) A review of recent research on the East Asian summer monsoon in China. Monsoon Meteorology. Oxford University Press,

Wang B, Wu R (1997a) Peculiar temporal structure of the South China Sea summer monsoon. Advances in Atmospheric Sciences 14 (2):177-192

Wang B, Wu R (1997b) Peculiar temporal structure of the south china sea summer monsoon. Advances in Atmospheric Sciences 14 (2):177-194. doi:10.1007/s00376-997-0018-9

Wentz FJ, Gentemann C, Smith D, Chelton D (2000) Satellite Measurements of Sea Surface Temperature Through Clouds. Science 288 (5467):847-850. doi:10.1126/science.288.5467.847

Wu R (2010) Subseasonal variability during the South China Sea summer monsoon onset. Climate Dynamics 34 (5):629-642. doi:10.1007/s00382-009-0679-4

Wu R, Kirtman BP, Pegion K (2006) Local Air–Sea Relationship in Observations and Model Simulations. Journal of Climate 19 (19):4914-4932. doi:doi:10.1175/JCLI3904.1

Wu R, Kirtman BP, Pegion K (2008) Local rainfall-SST relationship on subseasonal time scales in satellite observations and CFS. Geophys Res Lett 35 (22):L22706. doi:10.1029/2008gl035883

Wu R, Wang B (2000) Interannual variability of summer monsoon onset over the western North Pacific and the underlying processes. Journal of Climate 13 (14):2483-2501

Wu R, Wang B (2001) Multi-stage onset of the summer monsoon over the western North Pacific. Climate Dynamics 17 (4):277-289

Xie S-P, Chang C-H, Xie Q, Wang D (2007) Intraseasonal variability in the summer South China Sea: Wind jet, cold filament, and recirculations. J Geophys Res 112 (C10):C10008. doi:10.1029/2007jc004238

Xie S-P, Liu WT, Liu Q, Nonaka M (2001) Far-Reaching Effects of the Hawaiian Islands on the Pacific Ocean-Atmosphere System. Science 292 (5524):2057-2060. doi:10.1126/science.1059781

Xie S-P, Philander SGH (1994) A coupled ocean atmosphere model of relevance to the ITCZ in the eastern Pacific. Tellus A 46 (4):340-350

Xie S-P, Tanimoto Y (1998) A pan Atlantic decadal climate oscillation. Geophysical Research Letters 25 (12):2185-2188

Xie SP, Xie Q, Wang D, Liu WT (2003) Summer upwelling in the South China Sea and its role in regional climate variations. J Geophys Res 108 (3261):17-11

Yu L, Jin X, Weller RA (2008) Multidecade global flux datasets from the Objectively Analyzed Air–Sea Fluxes (OAFlux). Project: Latent and sensible heat fluxes, ocean evaporation, and related surface meteorological variables., vol OA-2008-01. Woods Hole Oceanographic Institution,

Zeng L, Wang D (2009) Intraseasonal variability of latent-heat flux in the South China Sea. Theoretical and Applied Climatology 97 (1):53-64. doi:10.1007/s00704-009-0131-z

Zheng Y, Waliser DE, Stern WF, Jones C (2004) The role of coupled sea surface temperatures in the simulation of the tropical intraseasonal oscillation. Journal of Climate 17 (21):4109-4134

Figure Captions

Figure 1. (a) Climatology of SST (colors; unit: °C) and surface winds (vectors) over SCS during April to July (1998-2009). Scaling of vectors (unit: ms^{-1}) is given on top of the figure. (b) Standard deviation of intraseasonal variability of SST (unit: °C) during the same period. Shading conventions are represented at the side of the figures.

Figure 2. Intraseasonal time series of SST (red, unit: °C) precipitation (grey, unit: mm day^{-1}) anomalies averaged over the inset rectangle in Fig. 1, from April-July, for the years 1998-2009. Scaling convention of SST (precipitation) is given on the left (right) x-axis. SST maximum events are defined as when the intraseasonal SST anomalies are above 1 standard deviation (horizontal dashed line, 0.242°C).

Figure 3. Lead-lag correlation of SST anomalies with respect to rainfall anomalies, on intraseasonal time scales averaged over the inset rectangle in Fig. 1. Maximum correlation (r=0.44, at 99% significance levels), is observed when SST anomalies lead the precipitation anomalies by 10 days.

Figure 4. Hovmoller plots of intraseasonal anomalies of (a) surface zonal wind (colors; unit: ms^{-1}), (b) surface latent heat flux (colors; unit: W m^{-2}), (c) downward shortwave radiation flux (colors; unit: W m^{-2}), (d) meridional sea level pressure gradient (colors;

unit: hPa/degree latitude), (e) surface air temperature (colors; unit: °C), (f) θ_e at 1000hPa (colors; unit: K) (g) $\Delta\theta_e$ (colors; unit: K) and (h) precipitation (colors; unit: mm day^{-1}) over the SCS (105-125°E), with respect to the SST maximum at day=0. Contour lines of SST anomalies (interval: 0.1°C) shown in are superimposed, with negative values dashed. Coloring convention is represented at the side of each panel.

Figure 5. Composites of intraseasonal SST (colors; unit: °C) and surface wind (vectors) anomalies with respect to the SST maximum are shown on the upper panel. Composites of intraseasonal precipitation (colors; unit: mm day^{-1}) and sea level pressure (contour lines; interval: 10Pa) anomalies during the same period are shown on the bottom panel. Scaling of vectors (unit: ms^{-1}) is given on top of the figure. Coloring convention is represented at the side of the figures.

Figure 6. A schematic figure of the active (red shades) – break (blue shades) intraseasonal cycle of precipitation over the SCS.

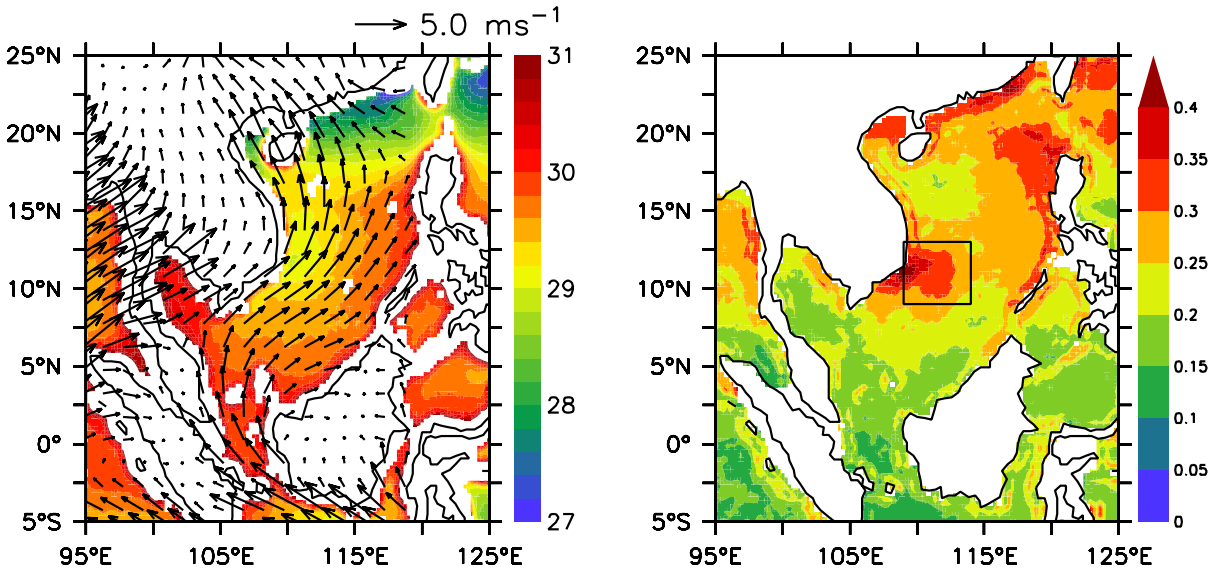

Figure 1. (a) Climatology of SST (colors; unit: °C) and surface winds (vectors) over SCS during April to July (1998-2009). Scaling of vectors (unit: ms^{-1}) is given on top of the figure. (b) Standard deviation of intraseasonal variability of SST (unit: °C) during the same period. Shading conventions are represented at the side of the figures.

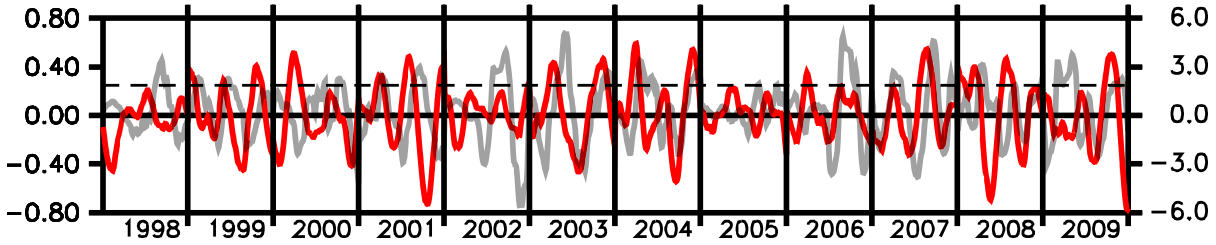

Figure 2. Intraseasonal time series of SST (red, unit: °C) precipitation (grey, unit: mm day^{-1}) anomalies averaged over the inset rectangle in Fig. 1, from April-July, for the years 1998-2009. Scaling convention of SST (precipitation) is given on the left (right) x-axis. SST maximum events are defined as when the intraseasonal SST anomalies are above 1 standard deviation (horizontal dashed line, 0.242°C).

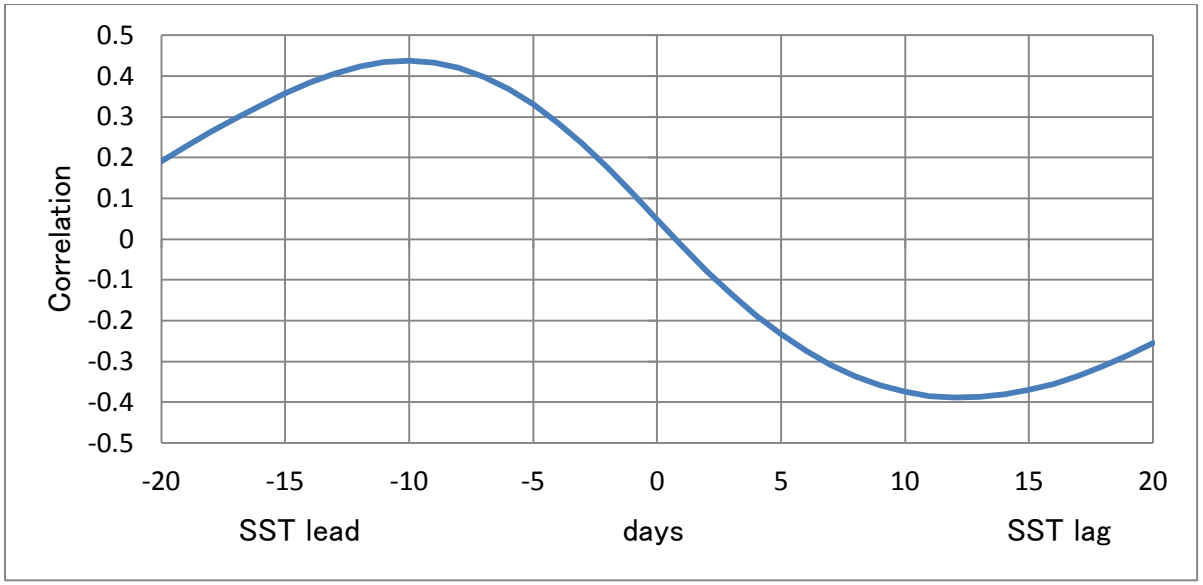

Figure 3. Lead-lag correlation of SST anomalies with respect to rainfall anomalies, on intraseasonal time scales averaged over the inset rectangle in Fig. 1. Maximum correlation (r=0.44, at 99% significance levels), is observed when SST anomalies lead the precipitation anomalies by 10 days.

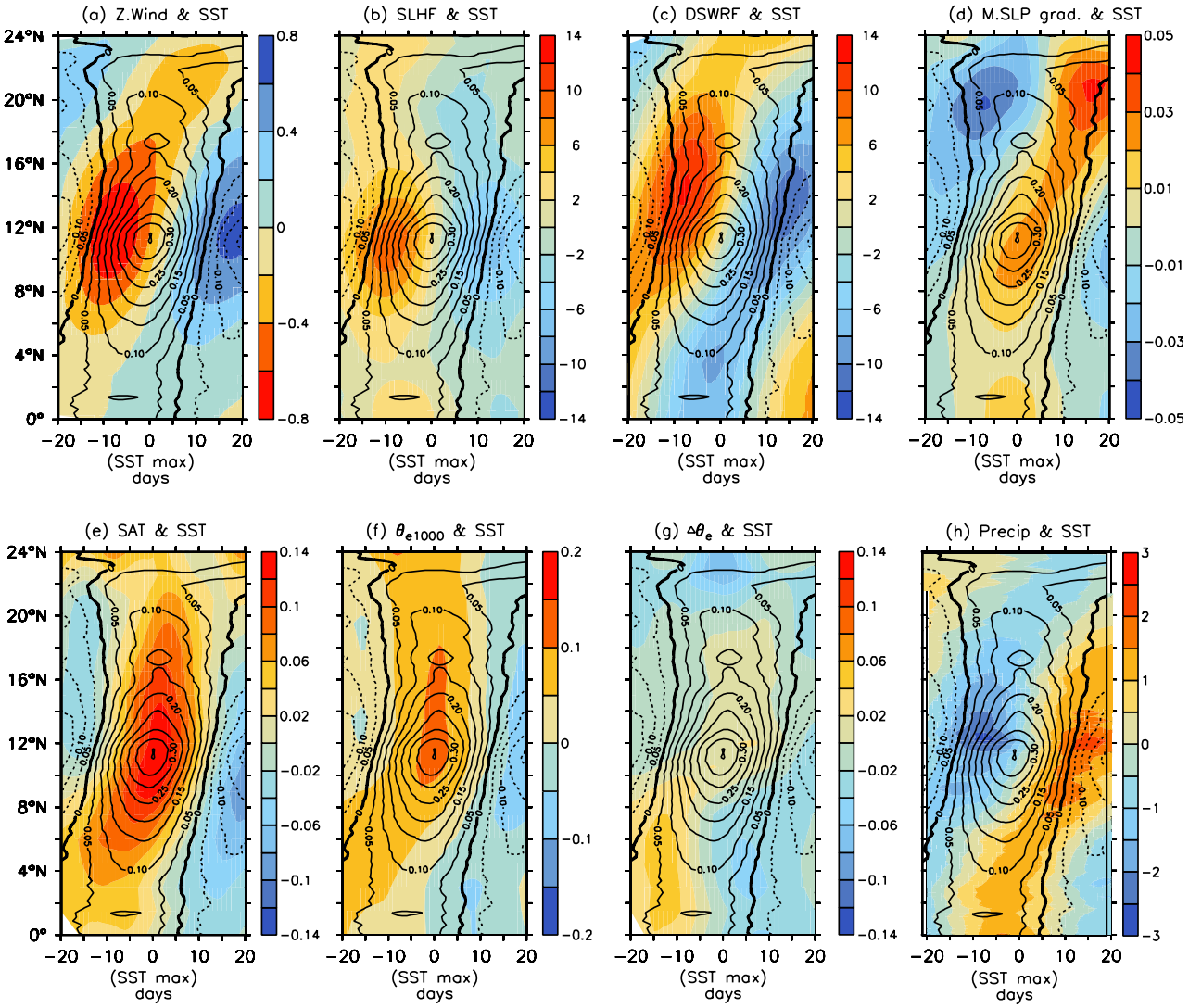

Figure 4. Hovmoller plots of intraseasonal anomalies of (a) surface zonal wind (colors; unit: ms^{-1}), (b) surface latent heat flux (colors; unit: W m^{-2}), (c) downward shortwave radiation flux (colors; unit: W m^{-2}), (d) meridional sea level pressure gradient (colors; unit: hPa/degree latitude), (e) surface air temperature (colors; unit: °C), (f) θ_e at 1000hPa (colors; unit: K) (g) $\Delta\theta_e$ (colors; unit: K) and (h) precipitation (colors; unit: mm day^{-1}) over the SCS (105-125°E), with respect to the SST maximum at day=0. Contour lines of SST anomalies (interval: 0.1°C) shown in are superimposed, with negative values dashed. Coloring convention is represented at the side of each panel.

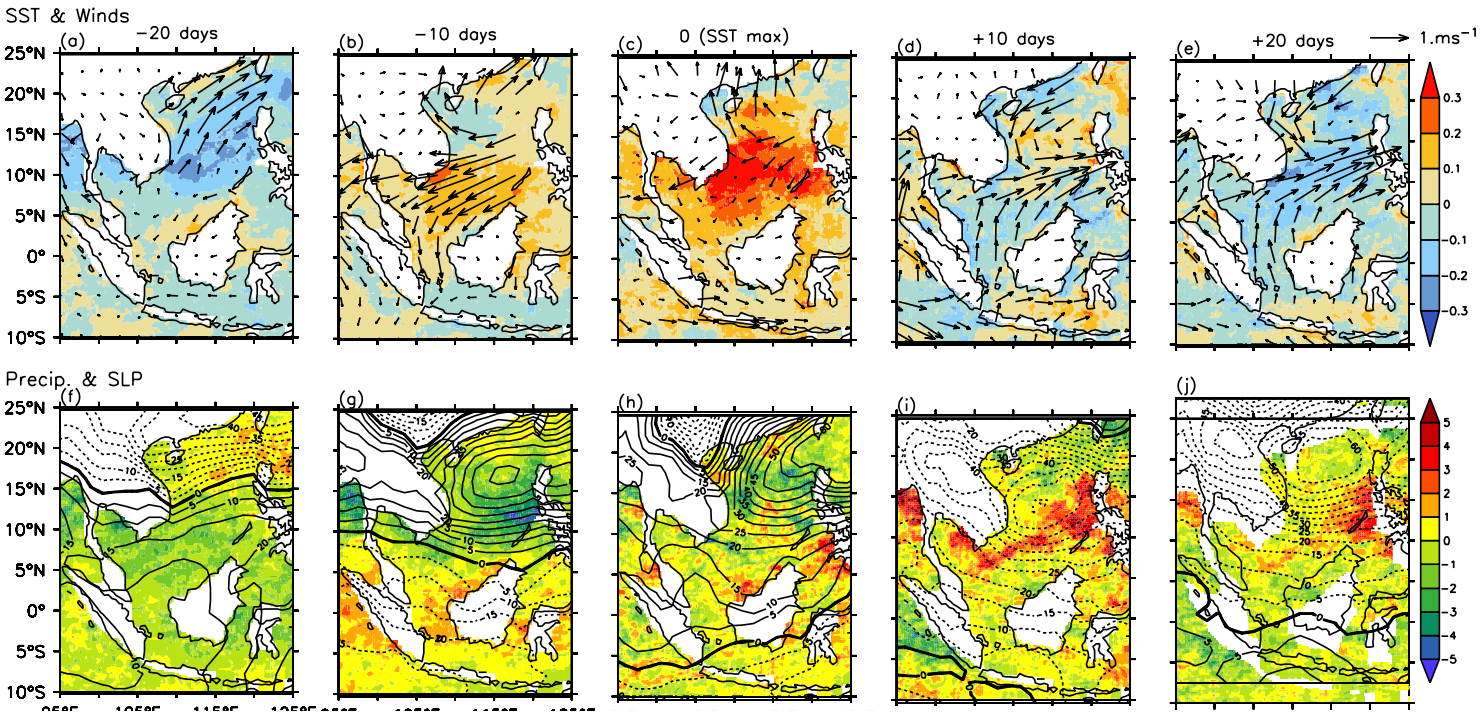

Figure 5. Composites of intraseasonal SST (colors; unit: °C) and surface wind (vectors) anomalies with respect to the SST maximum are shown on the upper panel. Composites of intraseasonal precipitation (colors; unit: mm day^{-1}) and sea level pressure (contour lines; interval: 10Pa) anomalies during the same period are shown on the bottom panel. Scaling of vectors (unit: ms^{-1}) is given on top of the figure. Coloring convention is represented at the side of the figures.

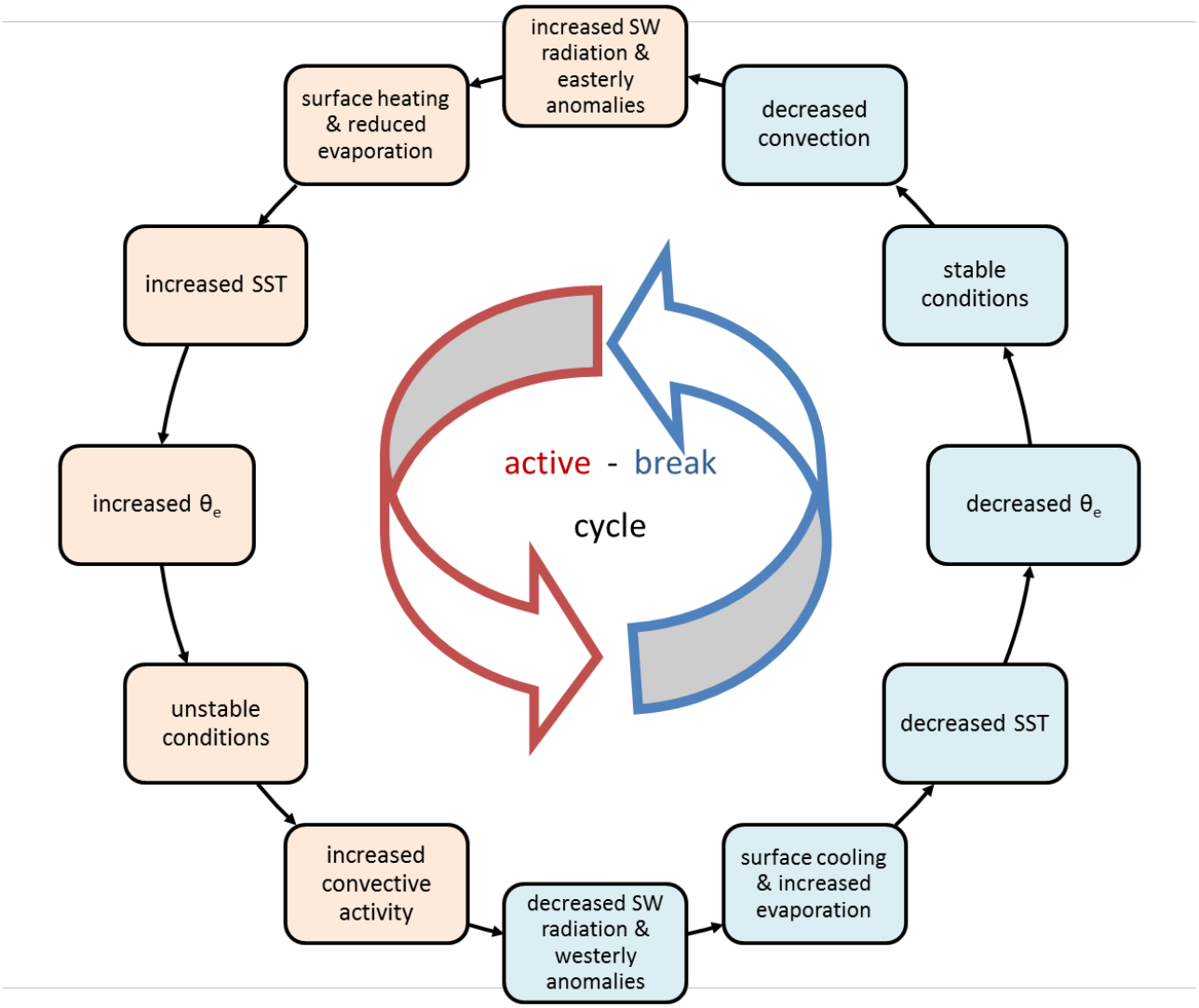

Figure 6. A schematic figure of the active (red shades) – break (blue shades) intraseasonal cycle of precipitation over the SCS.